# YIELDING OF 6061-T6 ALUMINUM TUBINGS UNDER DYNAMIC BIAXIAL LOADINGS

D. H. Y. NG, L. H. N. LEE
*University of Notre Dame, Department of Aerospace and Mechanical Engineering, Notre Dame, Indiana 46556, U.S.A.*

SUMMARY

A test vehicle for applying biaxial, tension-internal pressure, loading to thin-walled tubular specimens over a range of loading rates has been developed. The test vehicle consists of a housing, a number of pistons and three pressure chambers. Static axial and hoop stresses can be obtained and controlled independently. For additional dynamic loading, the dynamic piston assembly which produces internal pressure to the specimen is driven inward by an impact of a spherical pendulum. The dynamic stress path of the specimen is a part of the natural response of the system partially controllable through adjusting the initial static stress state and impact velocity.

Ten tubular specimens fabricated of 6061-T6 aluminum alloy were prepared. For comparison with dynamic responses, static initial and subsequent yield surfaces of the specimens have been obtained. The static yield surfaces were obtained by adopting Phillip's single-specimen probing approach. From a dynamic test, a set of dynamic stress-strain curves was constructed from the corresponding discrete values of stress and strain obtained from the measured pressure, strain vs. time curves at time intervals of 5 μs. By using a back extrapolating technique, the dynamic yield point was defined and located. It was found, in all three dynamic tests, dynamic yielding occurred at about 50-70 μs. At yielding, the corresponding hoop strain rate varied from 38.2/sec to 47.0/sec and the axial strain rate from -3.3/sec to 2/sec. The present dynamic yield strength exceeds the corresponding static yield strength by about 26%. The shape of the dynamic yield locus appears approximately to be a von Mises type. Furthermore, the strain rate vectors are in directions approximately normal to the dynamic yield surface. In addition, the stress path obtained in a dynamic biaxial test was reproduced statically. The corresponding stress-strain relationships have been compared and found significantly different.

An experimental and analytical study of the change in microstructure of the plastically deformed specimens was also performed. A probabilistic dislocation model having uniform, randomly-distributed glide plane orientations and Burgers vector directions was employed. The fundamental relation between the dislocation theory and continuum plasticity is that the continuum plastic strain rate is the sum of dislocation fluxes each of which is determined by the particular crystalline orientation tensor, magnitude of Burgers vector, mobile fraction, dislocation density and dislocation speed. Dislocation densities of the specimens at various stress states were obtained by the transmission electron microscopy. A comparison of the theoretical with experimental plastic strain rates was made. Some correlation was found.

## 1. Introduction

Theoretical and experimental investigations of material responses to dynamic loadings have been very active in the field of solid mechanics. In dynamic tests, strain rate is usually considered as a parameter which may have a range from 1/sec to as high as $10^6$/sec. For strain rates in the range of $10^4$/sec or higher, experimental techniques usually employed involve either a bar impact or a plate impact in which large amplitude and discontinuous stress or deformation waves propagate. Independent and simultaneous measurements of stress, strain and acceleration at the same material point are not possible. Thus, experimental data obtained for determining dynamic constitutive relationships usually require theoretical interpretations which may themselves include unproven, a priori assumptions for physical and mathematical simplifications. In the past, most wave propagating tests were limited to that of uniaxial stress or torsion. Only recently, Hsu and Clifton [1] and Lewis and Goldsmith [2] conducted tests with combined stresses.

Under uniaxial conditions, stress and strain data can be obtained by independent measurements. Here, two different techniques have been commonly used. The first technique utilizes the so-called Hopkinson pressure bar for uniaxial loading of short compression, tension or shear specimens. The second technique employs the uniform expansion of a thin-walled circular ring or tube [3-6]. The present paper describes a tension-internal pressure test vehicle designed to apply biaxial stresses in tubings at various loading rates up to 100/sec. The results of a series of biaxial dynamic and corresponding static tests producing identical stress paths in 6061-T6 aluminum tubings at room temperature are presented. For comparison, a uniaxial test as well as an initial yield surface test were conducted to provide the static properties of the material. However, there were still uncertainties such as the existence of corners and cross effects (change in yield strength in a direction normal to the direction of initial loading) in the yield surface. Therefore, a subsequent yield surface test was also performed to provide additional information on the static properties of the material. An analytical and experimental investigation of the change in micro-structure of the specimens was also made. Comparisons between the dynamic and static results on the initial yielding and subsequent failure of the tubings under biaxial stresses are presented.

## 2. Test Vehicle

The essential features of the test vehicle, made of steel, are shown in Fig. 1. It consists of a housing, a number of pistons and three pressure chambers filled with hydraulic oil. The test specimen, S, is attached to the two axial stressing pistons, B, which may move axially when a pressure is applied in Pressure Chamber 1. A static hoop stress in the specimen may be developed by applying a static pressure in Pressure Chamber 2, which may transmit through the hoop stressing piston, D, and the dynamic piston assembly, P1, P2, P3, and produce a pressure in Pressure Chamber 3. The magnitudes of static axial and hoop stresses in the specimen can be controlled independently within an accuracy of $\pm$ 1.4 x $10^4$ N/m$^3$ ($\pm$ 2 psi).

When the specimen is subjected to an initial static stress state, additional dynamic stresses may be produced by an impact. For dynamic loading, one of the two dynamic piston assemblies is driven inward by an impact of a steel spherical pendulum with the piston P3 while the other piston P3 and the outside housing F3 are held stationary. After the impact, the forward movement of the pendulum of a prescribed amount is allowed and the pendulum is stopped by an energy absorbing barrier not connected to the test vehicle. During the impact, the dynamic piston assembly, its parts, P1, P2 and P3, are rigidly fastened to each other, may

be separated momentarily from Hoop Stressing Piston D. The impact velocity of the pendulum may be controlled by adjusting its initial height of swing of a range zero to five meters. The impact momentum may be further adjusted by using a pendulum of a different mass. However, the transient axial and hoop stresses in the specimen can not be controlled independently. The additional dynamic stress path of the specimen is a part of the natural response of the entire system only partially controllable through adjusting the initial static stress state and impact velocity. The maximum allowable displacements and velocities of the various pistons of the test vehicle permit a maximum axial, or hoop strain of about 11% and a maximum strain rate of about 100.0/sec to develop in the specimen.

3. Specimen Preparation

Ten tubular specimens a length of about 17 cm, a diameter of about 2.54 cm and a wall thickness of about 0.32 mm were fabricated of 6061-T6 aluminum alloy of which some of the dynamic properties are available in the literature. A slightly tapered hollow arbor of a low melting point alloy (cerro alloy) was pressed lightly into the finished bore of the specimen in order to finish the outside diameter of the specimen. Very light cuts were taken during the process to minimize heat build up. After finishing machining, the specimens were immersed in boiling water to melt the arbor away. Since the wall thickness of the specimens were extremely thin, cold working of the material occurred during the process of machining. Therefore the mechanical properties of the finished 6061-T6 aluminum specimen differed from those listed in the materials handbook [7].

4. Measuring System and Approach

The measuring system consists of two static pressure gages (HEISE product, Solid Front-Model), two Kistler static-dynamic pressure transducers of model 606A and 603A installed in pressure chambers 1 and 3 respectively, four Ellis model BAM-1 strain gage bridge and transistorized amplifier-meters, two charge amplifiers, one Tektronix type 561A two-channel oscilloscope and one Tektronix type 565 fourchannel oscilloscope. A triggering circuit consisting of a proximity switch and a magnetic holding device was designed and built. After the steel pendulum was released from the magnetic holding device, it passed by the proximity switch which started the sweep of the oscilloscope traces of the various signals. Four Micro-Measurements made foil strain gages, two EP-08-350 DD-350 type mounted longitudinally and two EP-08-090 EG-350 type mounted circumferentially were installed in the mid-section of the specimen. All static strains were recorded and read on the BAM-1 amplifier-meters except those for yield surface probing tests. The static yield surface probing tests demanded better readability of strains. In yield surface probing tests, strain signals were amplified in the BAM-1 amplifier-meter first and read out on a digital volt-meter with an accuracy of $\pm$ 1 micro strain unit. Likewise, the dynamic strain signals were amplified in the BAM-1 amplifier-meters and then the oscilloscopes provided the records. Calibration of pressure transducers was accomplished by comparing data read on the static pressure gages and corresponding oscilloscope output. The rise time of the pressure transducer and accompanying measuring system was found to be within 5 μs, which was less than one less than one tenth of the rise time of a dynamic pressure, in Pressure Chamber 1 or 3 (in a range from 50 μs to 150 μs), obtained in the present dynamic tests. Therefore, the distortion of a pressure or strain signal was negligible.

5. Experimental Procedure

5.1 Static Tests

First of all, a specimen was employed to obtain a complete static uniaxial stress-strain relationship as shown in Fig. 2. Then a single specimen was utilized to obtain data points in the first quadrant of the $\sigma_x$ (axial stress) vs. $\sigma_\theta$ (hoop stress) stress space to establish an initial yield surface. The specimen was loaded biaxially along several stress paths through the interior towards the yield surface. Whenever a small deviation of a magnitude of 5-10 micro strain units off the elastic path was observed, the specimen was considered to reach the yield surface. Adopting Phillip's extrapolation technique, [8] the first quadrant of the initial yield locus in the two dimensional stress space was established. After the initial yield surface was determined, a single specimen was used to determine the subsequent yield surface. The testing procedures were basically similar to those in the initial yield surface test except the specimen was first prestressed substantially in the axial direction. The initial and subsequent yield surfaces are shown in Fig. 3.

5.2 Dynamic Tests

For determining dynamic constitutive relationships, it would be desirable to obtain direct and independent measurements of stresses and strains; otherwise, other physical measurements require analytical interpretations based on physical or mathematical assumptions. Up to now, however, this appears to be physically unattainable. In the present approach, it is assumed that the axial stress, $\sigma_x$, is given by

$$\sigma_x = \frac{P_1 A_1 - M_1 c \ddot{\varepsilon}_x \ell/2}{A_s} \tag{1}$$

where $P_1$ is the pressure in Pressure Chamber 1, $A_1$ is the effective area of Piston B, $\ell$ is the length of the thin-walled section of the specimen, $M_1$ is the combined mass of Piston B and the specimen mount C, $\ddot{\varepsilon}_x$ is the axial strain acceleration, $A_s$ is the cross-sectional area of the specimen and coefficient c is a constant to be experimentally determined. It is based on the assumptions that Piston B is rigid and has a maximum velocity much smaller than the axial and bending stress wave speeds of the specimen and that most of the deformation occurs in the threaded connection and in the thin-walled section of the specimen which may be considered as having a negligible mass as compared to that of Piston B. Furthermore, the thin-walled section of the specimen may deform plastically but the threaded connection remains elastic. The dynamic hoop stress $\sigma_\theta$ is given by

$$\sigma_\theta = \frac{P_3 R_i - m\ddot{\varepsilon}_\theta R_m^2}{t_s} \tag{2}$$

where $P_3$ is the pressure in Pressure Chamber 3, m is the mass per unit area of specimen wall, $\ddot{\varepsilon}_\theta$ is the hoop strain acceleration. $R_i$ and $R_m$ are the inner and mean radii of the specimen, respectively and $t_s$ is the wall thickness of the specimen.

To determine the coefficient c, a series of dynamic tests were conducted. The ballistic pendulum was dropped from heights which produced only elastic deformation of the specimen. Hooke's law is then valid and the following relationships must hold:

$$\sigma_x = \frac{E}{1-\nu^2} \quad (\varepsilon_x + \nu\varepsilon_\theta) \tag{3}$$

$$\sigma_\theta = \frac{E}{1-\nu^2} \quad (\varepsilon_\theta + \nu\varepsilon_x) \tag{4}$$

where E is the modulus of elasticity and $\nu$ is the Poisson's ratio. The axial stress calculated from eq. (3) should agree with that of eq. (1). Thus the coefficient c can be determined.

In a dynamic biaxial test, a specimen was first loaded statically to a certain state of stress inside the initial static yield surface. Then a ballistic pendulum of a 9.977 kg mass and hanging 3.658 meters above ground level was dropped and struck the dynamic piston assembly. The specimen was then deformed biaxially and dynamically at a changing strain rate. All dynamic pressure and strain signals were recorded in photographic form. By using eqs. (1) and (2), complete stress paths were obtained. In determining the dynamic yielding, it was found that there was no unique definition and Phillip's quasi-static approach could not be applied to a transient stress path. In the present investigation, the stress-strain relationship was constructed from the corresponding discrete values of stress and strain obtained from the stress and strain vs. time curves at time intervals of 5 μs. By joining the first two points deviated from the linear elastic stress-strain curve and extrapolating back to intercept the elastic line allows one to locate a point of interception which corresponds to a stress state defined here as a dynamic yield point.

For each dynamic biaxial test, a static test following the dynamic stress path was performed. A corresponding static stress-strain relationship was obtained. A comparison of the stress-strain relationships obtained from a set of dynamic and static tests with an identical stress history was made. The results are given as follows.

## 6. Experimental Results and Discussions

The records of dynamic strain and pressure signals were magnified, replotted and employed in determining the dynamic stress paths of three different tests. The dynamic stress path of Specimen D2SP2 is shown in Fig. 4. The width of a signal could cause an error of reading of $\pm$ 4%. Stresses, strains and strain rates are average values at the mid-section of a specimen. Strain rate and strain acceleration are calculated from the strain vs. time curve. It was found that the lateral inertia effect of the specimen wall on the hoop stress is negligible. A dominating influence on the dynamic hoop stress-strain relationship is the strain rate effect. The experimentally determined dynamic yield points and a corresponding dynamic yield locus for an average strain rate of 40.0/sec are shown in Fig. 5. In all tests, dynamic yielding occurred at about 0.05 - 0.07 millisecond. The three dynamic stress paths were reproduced statically up to the static fracture stresses of three specimens. Fig. 5 shows that the static yield point is much lower than the dynamic yield point. It was also observed that at the static yield point, the static strain increment vector is in a direction nearly normal to the static yield surface. It has also been observed that the dynamic fracture stress and strain exceed the dynamic yield stress and strain by a margin 1.62 times larger than that of the corresponding static results. Furthermore, the static fracture, a form of local instability initiated by a small variation in wall thickness or material property, is comparatively localized as compared to that of the corresponding dynamic fracture.

Fig. 2 shows that the uniaxial static stress-strain curve of the machined specimen has a lower proportional limit comparing to that of the same material in the handbook [7]. The reason for this difference is probably due to the effects of specimen preparation process and specimen size. The present measured static initial yield surface shown in Fig. 3 is in good agreement with von Mises criterion for yielding of isotropic materials. The experimental subsequent yield surface is found similar to those obtained by Hu and Bratt [9].

## 7. Micro-structural Properties

An analytical and experimental investigation of the change in micro-structure of the

specimen material was also made. A number of thin-foil wafers were removed from the fractured specimens and observed by a transmission electron microscope the changes in dislocation density and particle distribution of precipitates. The micrographs showed that the average dislocation density of the "no-stress" regions of the finished specimens was about $2.14 \times 10^8$ lines/cm$^2$. The average dislocation density in the fractured region of the specimen subjected to an uniaxial static stress was found to be $2.46 \times 10^9$ lines/cm$^2$ and the average of the dynamically fractured specimen D2SP2 was about $2.47 \times 10^9$ lines/cm$^2$. It appeared that the dislocation densities of the statically and dynamically fractured materials were of the same order of magnitude. The current approach did not allow the observation of the change in microstructure during dynamic yielding. However, the available information does indicate the following two facts. An increase in plastic strain is accompanied by an increase in dislocation density. The difference between the dynamic and static yield stresses is related to the dislocation speed and the rate of dislocation production.

A probabilistic dislocation model suggested by Kelley [10] was employed to determine the theoretical dynamic yield stresses of the specimens. The theoretical model involves a dislocation speed function which includes a number of parameters such as average initial dislocation density, average activation volume and free energy. The average activation volume and free energy, which are influenced by the short-range barriers, may be determined by the expressions given by Arsenault [11] and by the experimentally measured average distance between particles of precipitates. The theoretical dynamic yield stresses so determined were about 11% lower than the corresponding experimental values.

8. Remarks

Concerning dynamic yield points in Fig. 5, Hoge [6] found that the dynamic uniaxial proportional limit for 6061-T6 aluminum was about $2.90 \times 10^8$ N/m$^2$ (42 Ksi) at a strain rate of 28/sec or $3.10 \times 10^8$ N/m$^2$ (45 Ksi) at a strain rate of 65/sec which is about 25% or 28.6% higher than the static proportional limit. In the present dynamic test results, the average hoop strain rate was found to be around 40/sec at yielding. The present dynamic yield strength exceeds the corresponding static yield strength by about 26% which is in good agreement with Hoge's results. In addition, Perrone [12] also showed that the dynamic uniaxial yield stress calculated from his rate sensitive formula is about 28% higher than the static yield stress with strain rate of 40/sec for 6061-T6 aluminum alloy. The determined dynamic biaxial yield points clearly illustrate the strengthening effect of strain rate. The few measured dynamic yield points are reasonably close to a von Mises yield surface isotropically enlarged from the static one, as shown in Fig. 5. Furthermore, the plastic strain rate vectors, as indicated in Fig. 5, are in the directions nearly normal to the average dynamic yield surface. The theoretical dislocation model limited by the available micro-structural observations does give a qualitative prediction of the strengthening effect of strain rate on dynamic yield stress.

References

[1] Hsu, J.C.C. and Clifton, R.J., "Plastic Waves in a Rate Sensitive Material-II. Waves of Combined Stress," J. Mech. Phys, Solids, 22, 255-266 (1974).

[2] Lewis, J.L. and Goldsmith, W., "A Biaxial Split Hopkinson Bar for Simultaneous Torsion and Compression," Rev. Sci. Instrum., 44, 811-813 (1973).

[3] Clark, D.C. and Duwez, P.E., "The Influence of Strain Rate on Some Tensile Properties of Properties of Steel," Am. Soc. Testing Mater. Proc., 50, 560 (1950).

[4] Hoggatt, C.R., Orr, W.R. and Recht, R.F., "The Use of an Expanding Ring for Determining Tensile Stress-Strain Relationships as Functions of Strain Rate," The First International Conference of the High Energy Forming, Estes Park, June 19-23 (1967).

[5] Lindholm, U.S. and Yeakley, L.M., "A Dynamic Biaxial Testing Machine," Experimental Mechanics, 7, 1-7 (1967).

[6] Hoge, K.G., "Influence of Strain Rate on Mechanical Properties of 6061-T6 Aluminum under Uniaxial and Biaxial States of Stress," Experimental Mechanics, 2, 238-395 (1965).

[7] "Strength of Metal Aircraft Elements," Military Handbook MIL-HDBK-5 (1961).

[8] Phillips, A. Lin, C.S. and Justusson, J.W., "An Experimental Investigation of Yield Surfaces at Elevated Temperature," Acta Mechanica, 14, 119-146 (1972).

[9] Hu, L.W. and Bratt, J.F., "Effect of Tensile Plastic Deformation on Yield Condition," J. Appl. Mech, 25, 411 (1958).

[10] Kelly, J.M., "Dislocation Models in Continuum Laws," Constitutive Equations in Viscoplasticity, edited by K.C. Valanis, ASME, (1976).

[11] Arsenault, R.J., editor, "Treatise on Materials Science and Technology, Vol. 6. Plastic Deformation of Materials," Academic Press (1975).

[12] Perrone, N., "Inpulsively Loaded Strain Hardened Rate - Sensitive Rings and Tubes," Int. J. Solids Structures, 6, 1119-1132 (1970).

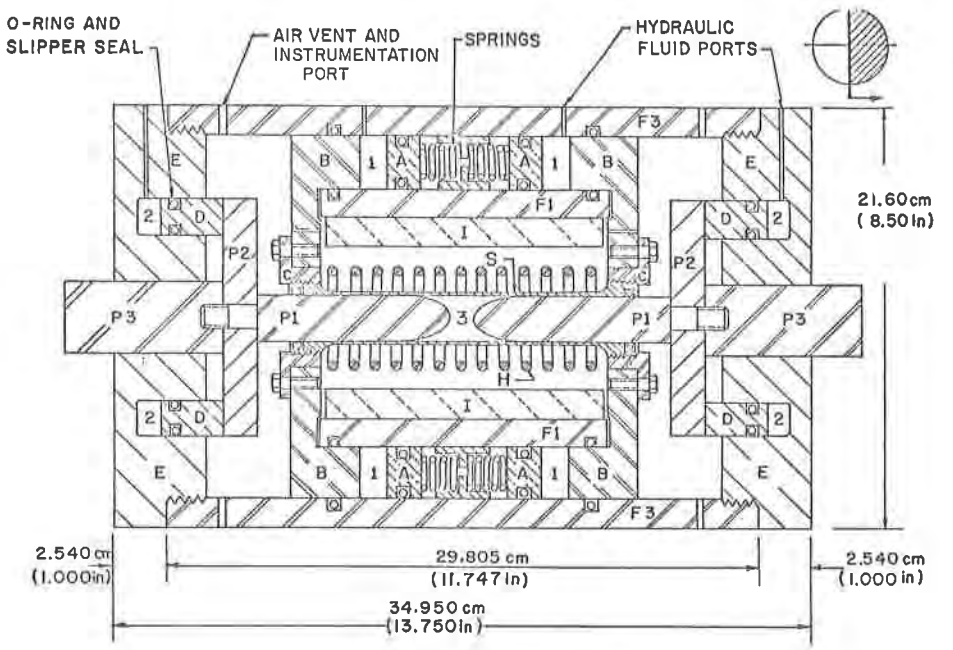


Fig. 1 Test vehicle

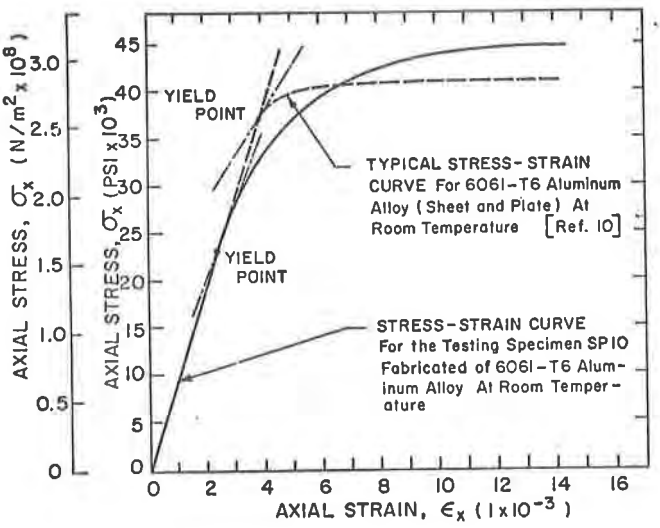


Fig. 2 Uniaxial static stress-strain curves of 6061-T6 aluminum alloy

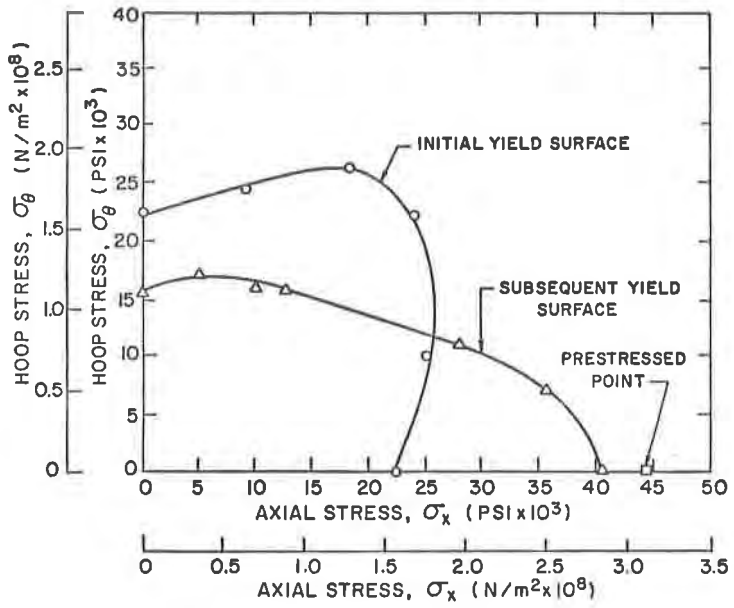


Fig. 3 Initial and subsequent static yield surfaces of 6061-T6 aluminum specimens

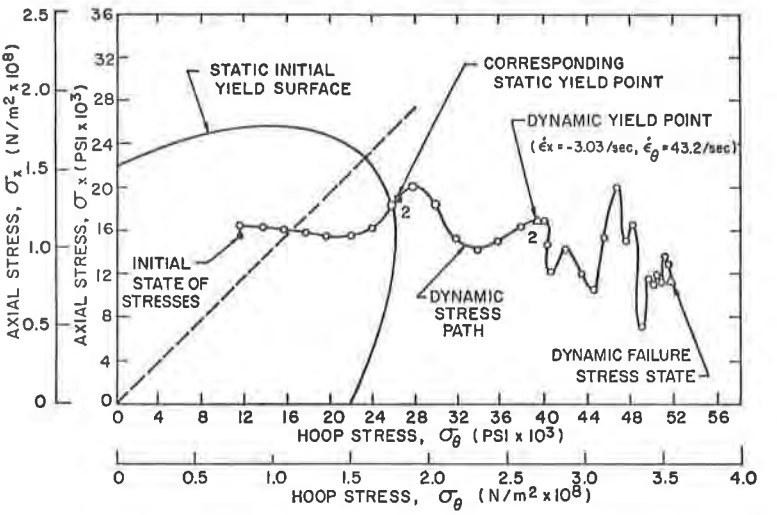


Fig. 4 Dynamic stress path of specimen D2SP2

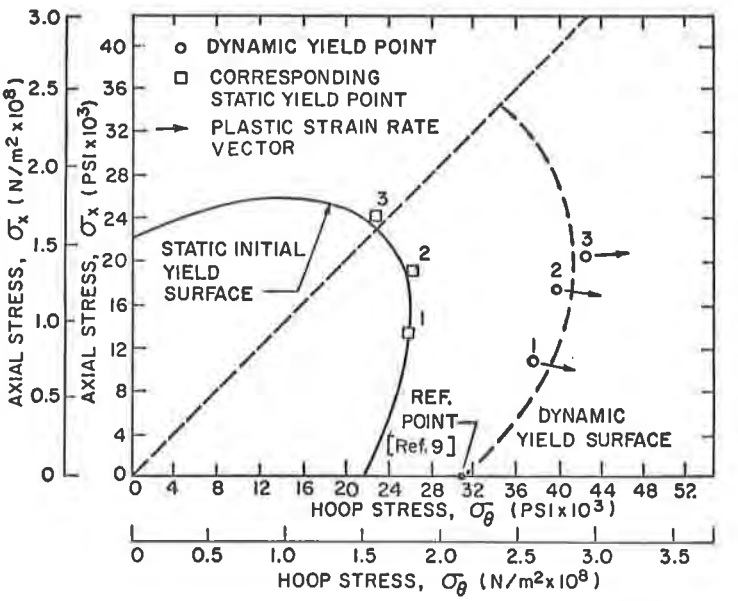


Fig. 5 Dynamic yield points and yield surface